ISSN 1674-1056
http://cpb.iphy.ac.cn
http://iopscience.iop.org/cpb
中国物理 B
Chinese Physics
中国物理 Chinese Physics B

Enhanced thermoelectric performance through homogenously dispersed MnTe nanoparticles in p-type $Bi_{0.52}Sb_{1.48}Te_3$ nanocomposites

Tian-Qi Lu(陆天奇), Peng-Fei Nan(南鹏飞), Si-Long Song(宋思龙), Xin-Yue Zhu(朱欣悦), Huai-Zhou Zhao(赵怀周), Yuan Deng(邓元)
Citation: Chin. Phys. B . 2018, 27(4): 047207. **doi:** 10.1088/1674-1056/27/4/047207

Journal homepage: http://cpb.iphy.ac.cn; http://iopscience.iop.org/cpb

What follows is a list of articles you may be interested in

Multinary diamond-like chalcogenides for promising thermoelectric application

Dan Zhang(张旦), Hong-Chang Bai(白洪昌), Zhi-Liang Li(李志亮), Jiang-Long Wang(王江龙), Guang-Sheng Fu(傅广生), Shu-Fang Wang(王淑芳)
Chin. Phys. B . 2018, 27(4): 047206. **doi:** 10.1088/1674-1056/27/4/047206

Biaxial strain-induced enhancement in the thermoelectric performance of monolayer WSe_2

Wanhuizi Shen(沈婉慧子), Daifeng Zou(邹代峰), Guozheng Nie(聂国政), Ying Xu(许英)
Chin. Phys. B . 2017, 26(11): 117202. **doi:** 10.1088/1674-1056/26/11/117202

Thermoelectric properties of Li-doped $Sr_{0.7}Ba_{0.3}Nb_2O_{6-\delta}$ ceramics

Ya-Cui Zhang(张亚翠), Jian Liu(刘剑), Yi Li(李宜), Yu-Fei Chen(陈宇飞), Ji-Chao Li(李吉超), Wen-Bin Su(苏文斌), Yu-Cheng Zhou(周昱成), Jin-Ze Zhai(翟近泽), Teng Wang(王腾), Chun-Lei Wang(王春雷)
Chin. Phys. B . 2017, 26(10): 107201. **doi:** 10.1088/1674-1056/26/10/107201

Unexpected low thermal conductivity and large power factor in Dirac semimetal Cd_3As_2

Cheng Zhang(张成), Tong Zhou(周通), Sihang Liang(梁斯航), Junzhi Cao(曹钧植),Xiang Yuan(袁翔), Yanwen Liu(刘彦闻), Yao Shen(沈瑶), Qisi Wang(王奇思),Jun Zhao(赵俊), Zhongqin Yang(杨中芹), Faxian Xiu(修发贤)
Chin. Phys. B . 2016, 25(1): 017202. **doi:** 10.1088/1674-1056/25/1/017202

Influences of spark plasma sintering temperature on the microstructures and thermoelectric properties of $(Sr_{0.95}Gd_{0.05})TiO_3$ ceramics

Li Liang-Liang, Qin Xiao-Ying, Liu Yong-Fei, Liu Quan-Zhen
Chin. Phys. B . 2015, 24(6): 067202. **doi:** 10.1088/1674-1056/24/6/067202

SPECIAL TOPIC — Recent advances in thermoelectric materials and devices

Enhanced thermoelectric performance through homogenously dispersed MnTe nanoparticles in p-type $Bi_{0.52}Sb_{1.48}Te_3$ nanocomposites*

Tian-Qi Lu(陆天奇)[1,2,†], Peng-Fei Nan(南鹏飞)[2,†], Si-Long Song(宋思龙)[1], Xin-Yue Zhu(朱欣悦)[3], Huai-Zhou Zhao(赵怀周)[2,‡], and Yuan Deng(邓元)[1,§]

[1] *School of Materials Science and Engineering, Beihang University, Beijing* 100191, *China*
[2] *Beijing National Laboratory for Condensed Matter Physics, Institute of Physics, Chinese Academy of Sciences, Beijing* 100190, *China*
[3] *Electronic Science and Technology, Beijing University of Posts and Telecommunications, Beijing* 102101, *China*

(Received 18 December 2017; revised manuscript received 25 December 2017; published online 10 March 2018)

In this work, we report that the thermoelectric properties of $Bi_{0.52}Sb_{1.48}Te_3$ alloy can be enhanced by being composited with MnTe nano particles (NPs) through a combined ball milling and spark plasma sintering (SPS) process. The addition of MnTe into the host can synergistically reduce the lattice thermal conductivity by increasing the interface phonon scattering between $Bi_{0.52}Sb_{1.48}Te_3$ and MnTe NPs, and enhance the electrical transport properties by optimizing the hole concentration through partial Mn^{2+} acceptor doping on the Bi^{3+} sites of the host lattice. It is observed that the lattice thermal conductivity decreases with increasing the percentage of MnTe and milling time in a temperature range from 300 K to 500 K, which is consistent with the increasing of interfaces. Meanwhile, the bipolar effect is constrained to high temperatures, which results in the figure of merit zT peak shifting toward higher temperature and broadening the zT curves. The engineering zT is obtained to be 20% higher than that of the pristine sample for the 2-mol% MnTe-added composite at a temperature gradient of 200 K when the cold end temperature is set to be 300 K. This result indicates that the thermoelectric performance of $Bi_{0.52}Sb_{1.48}Te_3$ can be considerably enhanced by being composited with MnTe NPs.

Keywords: MnTe nano particles, interface phonon scattering bipolar effect, higher engineering zT

PACS: 72.20.Pa, 73.50.Lw **DOI:** 10.1088/1674-1056/27/4/047207

1. Introduction

Thermoelectric materials can find their applications in direct conversion of heat to electric power or *vise versa* in solid state refrigeration with their performance being gauged by the figure of merit, $zT = \left(S^2\sigma/k\right)T$, where S is the Seebeck coefficient, σ is the electrical conductivity,k is the total thermal conductivity, and T is the absolute temperature.[1–4] To date, the enhancement of zT has been realized either by increasing the power factor ($S^2\sigma$), or by reducing the thermal conductivity k that consists of electrical part k_e and lattice part k_L, meanwhile avoiding the significant deterioration of the electrical conductivity. The approaches that can generally be used to improve the power factor include optimizing the carrier concentration, modifying the carrier mobility[5,6] or manipulating the carrier effective mass via band engineering.[7,8] On the other hand, the reduction of lattice thermal conductivity k_L can be attained through increasing phonon scatterings by multiple scale crystal defects, such as point defects, grain boundaries, intrinsic anharmonic phonons, etc.[9–12]

Bismuth–tellurium-based thermoelectric materials have been studied for several decades due to their exclusively superior performances at around room temperature. Although persistent efforts have been made to improve the zT values of these materials since the 1950s, the peak zT of commercial Bi_2Te_3 and its alloys remain to be around 1. As of now, most of the research on this material has focused on reducing the lattice thermal conductivity through various approaches, such as the superlattices,[13] nanostructures,[14] the fabrications of composites, and so on. Attractively in the p-type Bi_2Te_3/Sb_2Te_3 superlattice, Rama *et al.* reported that the lattice thermal conductivity k_L at room temperature is reduced enormously, leading to $zT \sim 2.4$ at 300 K.[15] With regard to the nanostructures, Bed *et al.* reported a peak zT of about 1.4 at 373 K achieved in p-type nanocrystalline BiSbTe bulk material,[16] Yi *et al.* achieved a peak zT of about 1.3 at a temperature of 373 K.[17] Furthermore, the nano-compositing approach is conducive to improving the thermoelectric performance and has been widely used in thermoelectric systems.

*Project supported by the National Natural Science Foundation of China (Grant Nos. U1601213 and 51472052) and the Funds from Institute of Physics, Chinese Academy of Sciences.

†These authors contributed equally to this work.
‡Corresponding author. E-mail: Hzhao@iphy.ac.cn
§Corresponding author. E-mail: dengyuan@buaa.edu.cn

© 2018 Chinese Physical Society and IOP Publishing Ltd

For instance, Wu *et al*. improved the thermoelectric properties of ZnO by mixing poly-paraphenylene (PPP) in 2015.[18] This method is also suitable for the system of bismuth telluride. Li *et al*. reported a nano-composite of BiSbTe with 1-vol% Cu_3SbSe_4 nanoinclusions, which attains a peak zT of 1.6 at 476 K.[19] Kim *et al*. achieved a peak zT of 1.38 for the incorporation of 4-wt% Ta_2O_5 NPs at room temperature.[20] In addition, our group have also demonstrated that the zTs in $Bi_{0.48}Sb_{1.52}Te_3$ can be significantly enhanced by adding $MnSb_2Se_4$ via synergistically reducing the lattice thermal conductivity and improving the electrical transport.[21] However, owing to the complex components in the BiSbTe/$MnSb_2Se_4$ composites, the mechanism of the enhanced TE performance is yet to be clarified. Particularly, how the $MnSb_2Se_4$ can be decomposed into the relevant MnSe and Sb_2Se_3, and what the influence is of MnSe or similar MnTe nanoinclusions on the electrical property of BiSbTe still remains to be investigated.

In this work, the $Bi_{0.52}Sb_{1.48}Te_3$ based composites incorporated with MnTe nanoparticles are fabricated via ball milling (BM) and the SPS process. We attempt to optimize the total thermoelectric performance in the whole temperature range through adjusting the milling time and quantity of nanoparticles. The $Bi_{0.52}Sb_{1.48}Te_3$/2-mol% MnTe composite sample which underwent 3-h BM shows a remarkable decrease in lattice thermal conductivity and enhancement of power factor (PF) at high temperature. According to the result, we propose that most of the MnTe naonparticles are dispersed uniformly and form secondary phases to affect the properties of $Bi_{0.52}Sb_{1.48}Te_3$, meanwhile, partial Mn^{2+} ions from MnTe would substitute the Bi^{3+} or Sb^{3+} in the host $Bi_{0.52}Sb_{1.48}Te_3$, leading to increased hole concentration and enhanced electrical conductivity. As a result, the zT peak shifts toward higher temperature, the zT curves broaden, and the engineering zT is 20% higher than that of the pristine sample for the 2-mol% MnTe added composite at a temperature gradient of 200 K when the cold end temperature is set to be 300 K.

2. Experimental methods

2.1. Synthesis

Firstly, $Bi_{0.52}Sb_{1.48}Te_3$ was prepared by directly ball milling the pure elements Bi (chunks, 99.99%) , Sb (chunks, 99.999%), and Te (chunks, 99.999%) in a stainless steel jar with a high-energy ball mill machine, SPEX 8000D, and the pure materials were sealed into the jar in an argon-filled glove box. The sample was milled for 9 h and then pressed by the SPS process under an axial pressure of 40 MPa at 673 K for 5 min with a heating rate of 50 K/min. Similarly, the pure MnTe was fabricated by using the same method, but the milling time was changed to 6 h and the SPS process parameter was transformed into an axial pressure of 45 MPa at 1173 K for 30 min with a heating rate of 50 K/min. Secondly, $Bi_{0.52}Sb_{1.48}Te_3$ was incorporated independently with 0-mol%, 1-mol%, 2-mol%, and 4-mol% MnTe, for 10 min and 3 h, respectively through the ball milling process, then the mixed powders were put into a graphite die and pressed at 673 K for 5 min under 40 MPa again, respectively. Finally, these disk-shaped samples each with a diameter of 12.7 mm$\sim$ 2 mm in thickness, and relative densities of 97% were polished and cut for the characterizing and measuring the TE properties.

2.2. Measurements

2.2.1. X-ray diffraction

The phase analysis was performed by x-ray diffraction (Xpert Pro PANalytical XRD) using a Cu–Kα radiation (λ = 1.5418 Å) and operating under 40 kV and 40 mA. The patterns were obtained in a 2θ range of 10°–60° in steps of 0.02° at room temperature in air.

2.2.2. Microstructure analysis

The morphologies of bulk samples were characterized by scanning electron microscopy (SEM) on the S-5200 field emission SEM (Hitachi). The microstructure and second-phase particles in the bulk samples were investigated by using a transmission electron microscope (TEM, JEM-2100 Plus).

2.2.3. Hall measurements

The room-temperature Hall measurement was performed on a Nanometrics Hall Instrument. Samples were loaded with a BN substrate. Four probes were attached to the edge of the sample. The sample was placed in a vacuum with a magnetic field (up to $\pm$0.5 T) perpendicular to its surface. The resistivity ρ and Hall coefficient $R_{\rm H}$ (along the in-plane direction) were measured by the Van de Pauw method. The effective carrier concentration ($n_{\rm H}$) was calculated from the relationship $n_{\rm H} = 1/eR_{\rm H}$, where e is the elemental charge and $R_{\rm H}$ is the Hall coefficient. The Hall mobility ($\mu_{\rm H}$) was calculated from the relationship $\mu_{\rm H} = R_{\rm H}/\rho$.

2.2.4. Electrical properties

The obtained SPS pellets were cut into bars with dimensions 10 mm×3 mm×2 mm, and Seebeck coefficient and electrical conductivity of the dimensions were simultaneously measured from room temperature to 498 K under a low-pressure helium atmosphere by using LSR-3 equipment (Linseis, Germany).

2.2.5. Thermal conductivity

The thermal conductivity was calculated from $\kappa = D \cdot C_{\rm p} \cdot d$, where the thermal diffusivity coefficient (D) was measured

using the laser flash diffusivity method in a Linseis LFA-1000, the samples coated with carbon were placed into the mould and measured under flowing helium atmosphere from room temperature to 498 K; the density (d) was determined by using the Archimedes drainage method.

3. Results and discussion

3.1. Structure and morphology analysis

The room temperature XRD patterns for $Bi_{0.52}Sb_{1.48}Te_3$ composites added with 0, 1, 2, and 4 mol% of MnTe through ball milling (for 10 minutes and 3 hours, respectively) and SPS process are shown in Figs. 1(a) and 1(b). It can be seen that all the samples are of pure phase that can be indexed to the hexagonal crystal structure (space group, R-3mH). The secondary phases are difficult to detect because of the limit of instrument sensitivity. Figures 1(c) and 1(d) illustrate the changes of lattice constant along the a and c axes. The results for the 2-mol% MnTe sample (3 h) are abnormal because of the error in measurement. In general, it is obvious that the lattice constant enlarges slightly with MnTe content increasing, which might be due to the substitution of Mn atom (161 pm of atomic radius) on the Bi (143 pm) site.

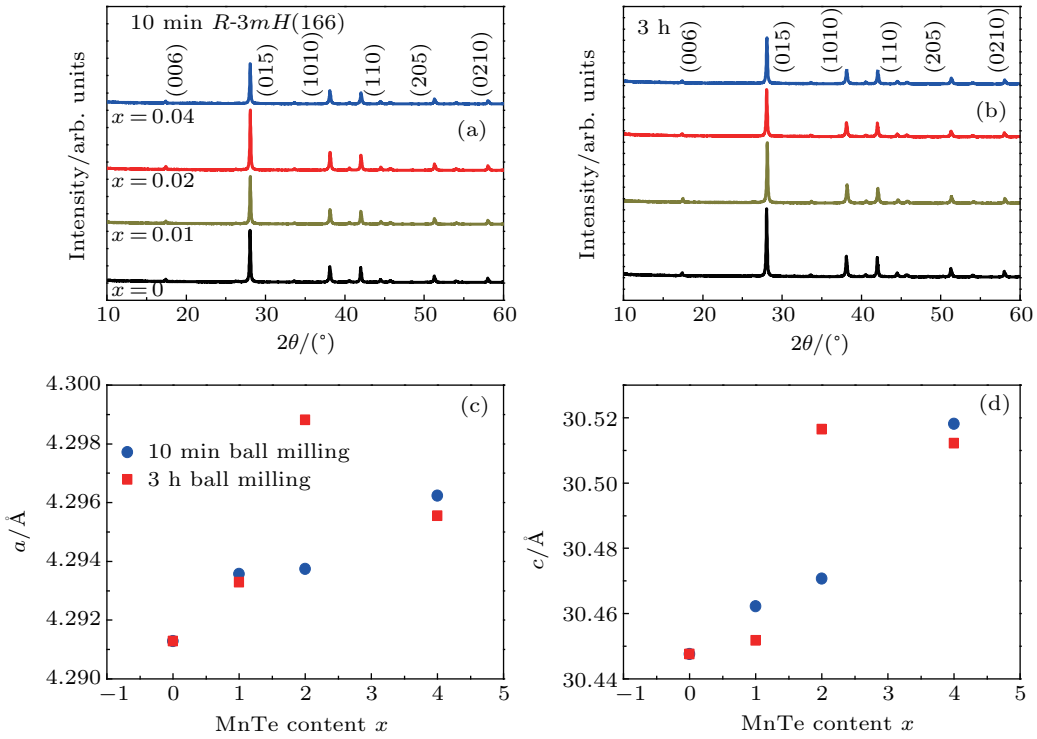


Fig. 1. (color online) X-ray diffraction patterns for $Bi_{0.52}Sb_{1.48}Te_3$ composites obtained by adding x-mol% MnTe milled (a) 10 min, (b) 3 h; (c) lattice parameters a and (d) lattice parameters c versus MnTe content, calculated by the Rietveld method for $Bi_{0.52}Sb_{1.48}Te_3$ compounds.

The low-magnification SEM image of $Bi_{0.52}Sb_{1.48}Te_3$ composites with 2-mol% MnTe prepared by 3-h ball milling plus SPS process is displayed in Fig. 2(a), in which we can observe homogeneous particles at around the 3 micrometer size. Figure 2(b) shows the high-magnification SEM image of the sample in which the lamellar structure of $Bi_{0.52}Sb_{1.48}Te_3$ can be clearly seen. The bright-field TEM image in Fig. 2(c) exhibits that the particles are made up of substantial nanoscale grains, indicating that a large number of interfaces exist in the samples. Figure 2(d) shows the high magnification TEM image of the marked part in Fig. 2(c), and it shows the grain boundaries and grains on the order of $\sim$ 20 nanometers clearly. In the inset of Fig. 2(d), the analysis of interplanar spacing confirms that this annotated grain is of the second phase of MnTe, which is consistent with the preliminary composite

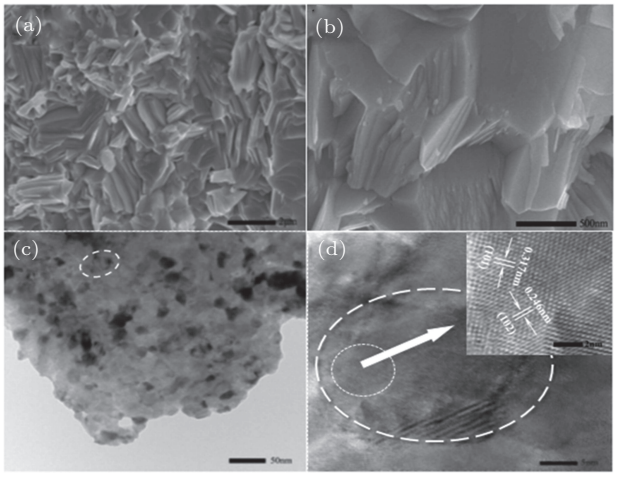


Fig. 2. (a) Low-magnification SEM images; (b) high-magnification SEM images; (c) bright-field TEM image; (d) HRTEM image of the marked part in panel (c), the inset shows the locally enlarged drawing of $Bi_{0.52}Sb_{1.48}Te_3$ composites (2-mol% MnTe milled 3 h).

3.2. Thermal and electrical transport properties

3.2.1. Thermal transport properties

Figure 3(a) displays the thermal diffusion coefficients as a function of temperature for a series of $Bi_{0.52}Sb_{1.48}Te_3$ composites. It shows an obvious rising trend at low temperature but a suppressed bipolar effect with the increasing of doping concentration. Meanwhile, with the increasing of ball milling time, the thermal diffusion coefficients decrease significantly, which can be ascribed to the refined grain sizes of the composites, leading to the number of interfaces increasing and the heat carrying phonon scattering strengthening. Figure 3(b) exhibits the total thermal conductivities of the composites. As can be seen, the total thermal conductivities κ_{tot} have a similar trend to the thermal diffusion coefficients. κ_{tot} is the sum of the electrical (κ_{ele}) and lattice thermal conductivity (κ_{lat}). The value of κ_{ele} is estimated through the Wiedemann–Franz law $\kappa_{ele} = L\sigma T$, where L is the Lorentz number,[22] andcan be easily calculated in a system dominated by one type of electrical transport carrier, based on the SPB model using the following equations:[23]

$$L = \left(\frac{k_B}{e}\right)^2 \frac{(1+\lambda)(3+\lambda)F_\lambda(\eta)F_{2+\lambda}(\eta) - (2+\lambda)^2 F_{1+\lambda}(\eta)^2}{(1+\lambda)^2 F_\lambda(\eta)^2},$$
$$F_j(\eta) = \int_0^\infty f\xi^j \mathrm{d}\xi = \int_0^\infty \frac{\xi^j}{1+e^{(\xi-\eta)}}\mathrm{d}\xi. \quad (1)$$

Here, λ is the scattering factor and the $\lambda = 0$ for acoustic phonon scattering.[24] $F_j(\eta)$ is the Fermi integral, η is the reduced chemical potential defined as $\eta = (E_V - E_F)/(k_B T)$, where E_V is the energy of the valence band top and is the chemical potential. However, it is difficult to obtain it with the involvement of the so-called bipolar effect, by which minority carriers begin to contribute significantly to the electrical conductivity. Thus L is roughly calculated using an SPB with acoustic phonon-dominated scattering. In this study, L is obtained from the broadly adopted approach to fitting the Seebeck coefficient to the reduced chemical potential[25,26] (Fig. 3(c)). The results of the lattice thermal conductivities and bipolar thermal conductivities are shown in Fig. 3(d). The bipolar effect leads to an extra thermal conductivity, which results in an abnormally large lattice thermal conductivity above 400 K; this phenomenon weakens with doping amount increasing. Moreover, the lattice thermal conductivities show continuous decline with the gradual increase in MnTe percentage and milling time, which is in accord with the increasing of grain boundaries and phonon scattering.

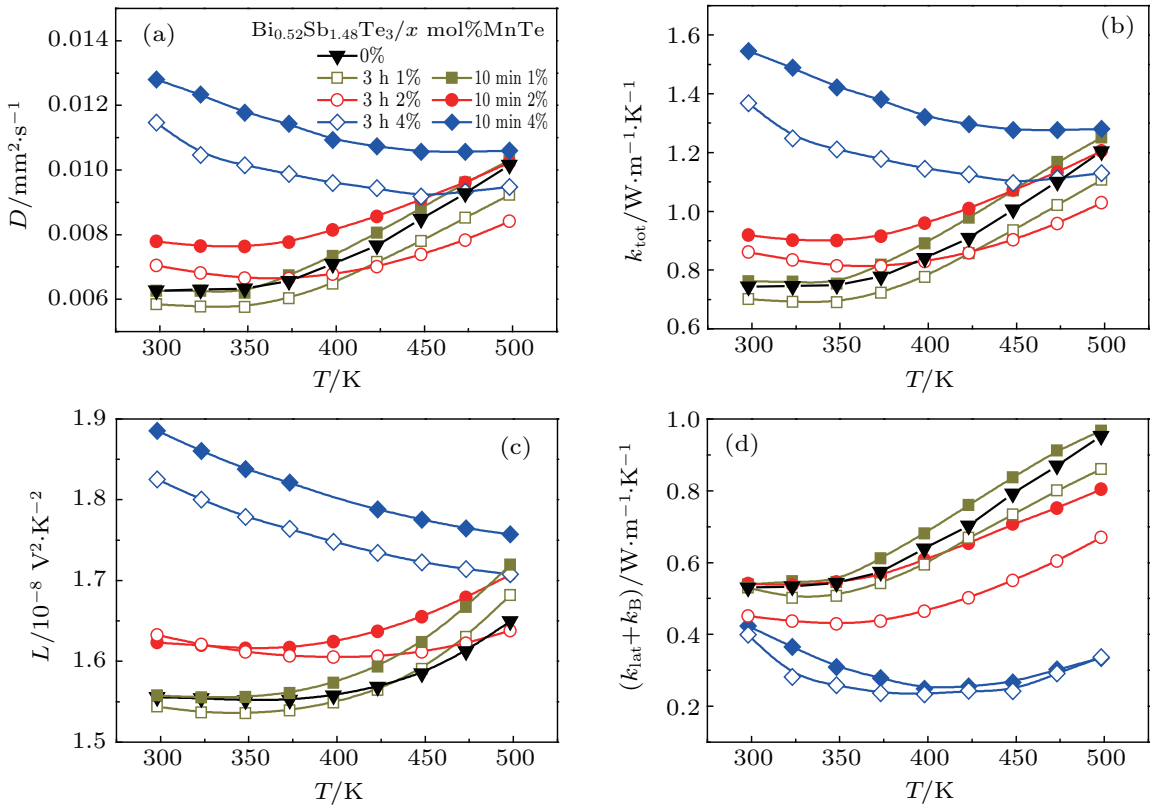


Fig. 3. (color online) Thermal properties as a function of temperature: (a) thermal diffusivities (D); (b) total thermal conductivities (κ_{tot}); (c) Lorenz numbers (L); (d) lattice thermal conductivities (κ_{lat}) and bipolar thermal conductivities (κ_b) for $Bi_{0.52}Sb_{1.48}Te_3$ compounds.

3.2.2. Electrical transport properties

In order to understand the influence of the MnTe additives on the electrical properties of $Bi_{0.52}Sb_{1.48}Te_3$ composites, Hall measurements are carried out for all the samples at room temperature. Figure 4(a) reveals that the carrier concentration goes up with increasing the MnTe content and is unrelated to the milling time. This can be explained as that the partial Mn^{2+} acceptor substitutes for the Bi^{3+} sites of the host lattice in the SPS process. At the same time, the carrier mobility decreases gradually as shown in Fig. 4(b), indicating that the scattering of electrons by nano-particles of the second phase strengthens. The experimental data of $Bi_{0.52}Sb_{1.48}Te_3$ composites can be analyzed on the basis of the Boltzmann transport equation within the relaxation time approximation. In Fig. 4(c), the Pisarenko line was plotted based on a single parabolic band (SPB) model, where the relationship between Seebeck and carrier concentration can be expressed as[27,28]

$$S = \frac{k_B}{e}\left(\frac{(2+\lambda)F_{\lambda+1}(\eta)}{(1+\lambda)F_\lambda(\eta)} - \eta\right), \tag{2}$$

$$n_H = 4\pi\left(\frac{2m^* k_B T}{h^2}\right)^{3/2} F_{1/2}. \tag{3}$$

Here, k_B, e, λ, h, and m^* are the Boltzmann constant, electron charge, the scattering factor, Planck constant, and effective mass, respectively. The acoustic phonon scattering with $\lambda = 0$ is generally accepted as the dominant scattering mechanism in limiting the carrier mean free path.[24,29] Thus, the effective mass $m^* = 1.5m_e$ can be obtained for the $Bi_{0.52}Sb_{1.48}Te_3$ sample at room temperature. On the assumption that the effective mass does not change in other samples, the value of S can be calculated according to the carrier concentration. In Fig. 4(c), it can be seen that at 300 K the experimental Seebeck coefficients rise by about 7, 5, and 22 μV/K for those 3-h ball milling samples, and 13, 20, and 36 μV/K for 10-min samples compared with the calculated results given by the model, which will be beneficial to the electrical power factors of the composites.

The temperature-dependent electrical conductivities for a series of samples with various MnTe content are shown in Fig. 5(a). It can be seen that the electrical conductivity increases significantly with MnTe content, resulting from the higher carrier concentration caused by the doping effect of Mn atoms on Bi sites. Figure 5(b) displays the temperature dependent Seebeck coefficients of the series of samples. The substantial reduction of Seebeck coefficient for each of the composite samples is also ascribed to the increase of carrier concentration. Apart from the 4-mol% samples, others display the bipolar effects above 400 K. It is worth mentioning that all the samples that have undergone 3-h ball milling have larger Seebeck coefficients than those of 100-min milling samples.

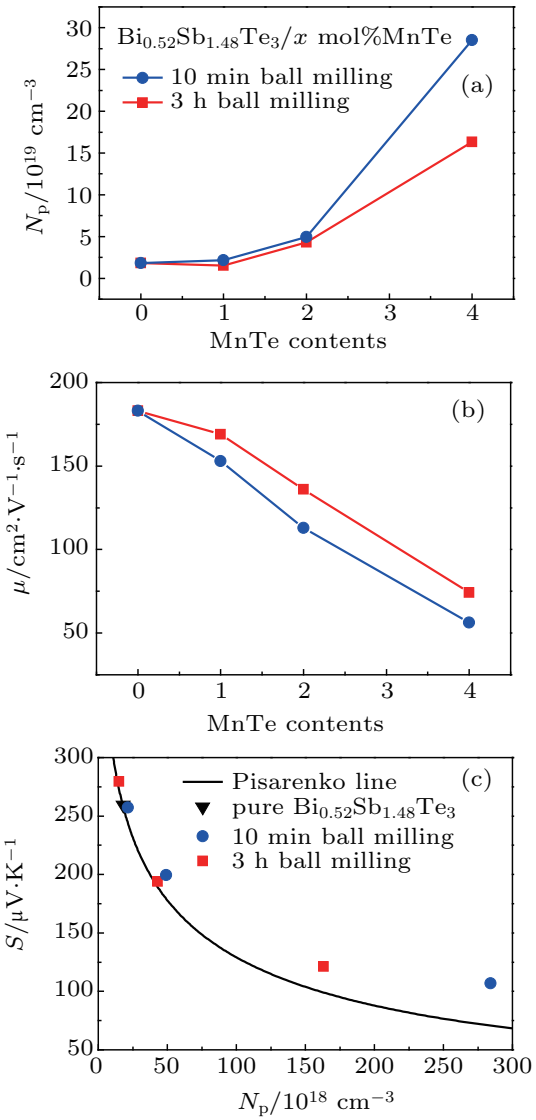


Fig. 4. (color online) (a) Room temperature carrier concentration (N_p) and (b) room temperature carrier mobility (μ_H) as a function of MnTe contents (x); (c) Pisarenko relation given by the black solid line under the assumption of a single parabolic band model at room temperature compared with the estimated results given by the mode on compounded samples.

Figure 5(c) shows the temperature-dependent power factors. The 2-mol% MnTe sample undergoing 3-h ball milling has a superior power factor than the pristine $Bi_{0.52}Sb_{1.48}Te_3$ sample over the whole temperature range. The power factor of the 4-mol% sample is larger than that of the pristine sample only above 373 K. The dimensionless thermoelectric figures of merit zT as a function of temperature are presented in Fig. 5(d). The zT obtained from the 1-mol% MnTe sample is the highest in zT values of all MnTe samples and its peak value reaches 1.37 at 348 K, which is 10.4% higher than that for the pristine sample. For the 2-mol% MnTe sample undergoing 3-h ball milling, though the zT is reduced slightly from room temperature to 348 K with respect to zT value the pure $Bi_{0.52}Sb_{1.48}Te_3$, it possesses a better thermoelectric performance from 373 K to 498 K.

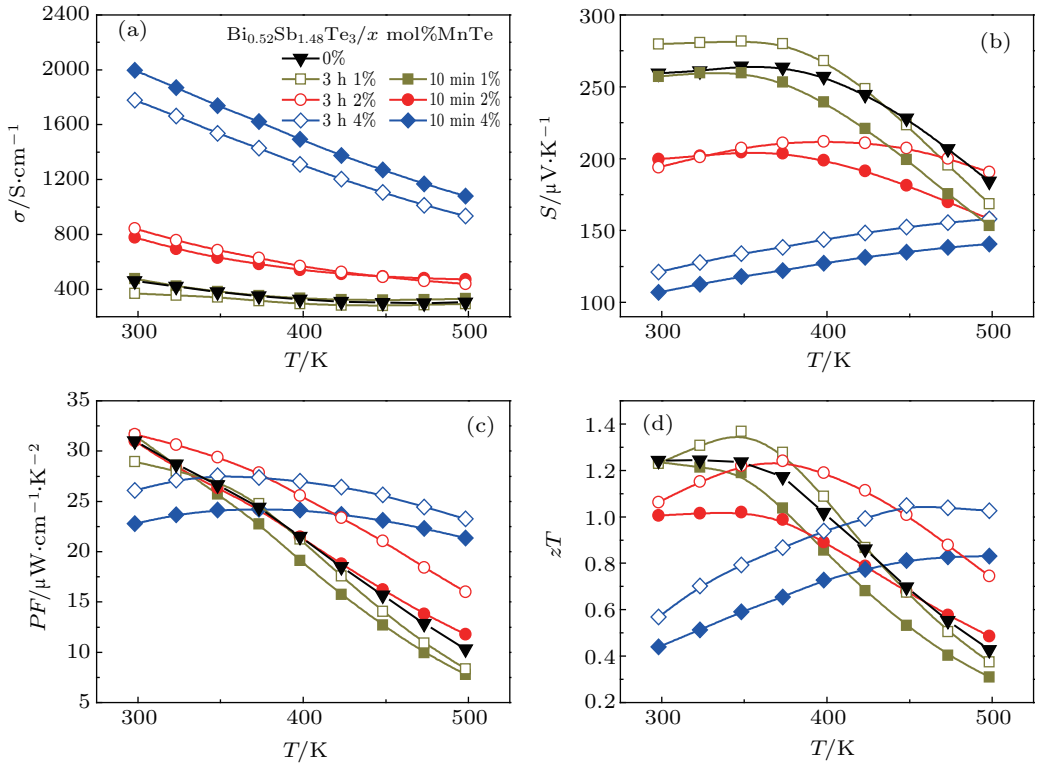


Fig. 5. (color online) Temperature dependence of thermoelectric properties. (a) Electrical conductivity, (b) Seebeck coefficient, (c) power factor, and (d) zT values for $Bi_{0.52}Sb_{1.48}Te_3$ compounds.

3.3. Actual thermal efficiency

To effectively assess the desirability of materials for thermoelectric applications, Kim *et al*. defined the engineering power factor $(PF)_{eng}$ and engineering dimensionless figure of merit $(zT)_{eng}$ to accurately predict the energy conversion efficiency (η) and output power density (P_d) of materials other than using conventional average zT values.[30] The $(PF)_{eng}$ and $(zT)_{eng}$ can be given by

$$PF_{eng} = \frac{\left(\int_{T_c}^{T_h} S(T)\,dT\right)^2}{\int_{T_c}^{T_h} \rho(T)\,dT}, \tag{4}$$

$$zT_{eng} = \frac{PF_{eng}}{\int_{T_c}^{T_h} k(T)\,dT}\Delta T. \tag{5}$$

Here, T_h, T_c, and ΔT are the hot-side temperature, the cold-side temperature, and the temperature difference between both sides, respectively. Figure 6(a) displays the temperature difference ΔT dependence of $(PF)_{eng}$ for all the samples, showing improvement with increasing the MnTe and milling time. Figure 6(b) shows the ΔT dependence of $(zT)_{eng}$ of all samples. All samples undergoing 3-h ball milling have higher $(zT)_{eng}$ than those with 10-min milling, and among them the $(zT)_{eng}$ of the 2-mol% MnTe sample reaches 0.54 when the ΔT is 200 K, which is nearly 20% higher than that of the pure $Bi_{0.52}Sb_{1.48}Te_3$.

The concept of maximum efficiency was first proposed by Altenkirch in 1909 to measure the actual power generation efficiency of a TE generator.[31] Subsequently, Kim *et al*.[30] put forward the output power density (P_d) to better reflect the comprehensive performance of a thermoelectric device, the output power density depends on the TE leg dimension and the material property whereas the maximum efficiency is dependent only on the material characteristics. The maximum efficiency (η_{max}) and output power density (P_d) based on cumulative temperature are derived as

$$\eta_{max} = \eta_c \frac{\sqrt{1+zT_{eng}(\hat{a}/\eta_c - 1/2)} - 1}{\hat{a}\left(\sqrt{1+zT_{eng}(\hat{a}/\eta_c - 1/2)} + 1\right) - \eta_c}, \tag{6}$$

$$P_d = \frac{PF_{eng}\Delta T m_{opt}}{L\left(1+m_{opt}\right)^2}, \tag{7}$$

where η_c is the Carnot efficiency and $\hat{a}$ is the dimensionless intensity factor of the Thompson effect, which is defined as follows:

$$\hat{a} = \frac{S(T_h)\Delta T}{\int_{T_c}^{T_h} S(T_h)\,dT}, \tag{8}$$

where $S(T_h)$ is the Seebeck coefficient at the hot-side temperature (T_h). Figures 6(c) and 6(d) show the cumulative temperature dependence of maximum efficiency (η_{max}) and output power density (P_d). The maximum efficiency of 1-mol% sample outperforms that of the pristine $Bi_{0.52}Sb_{1.48}Te_3$; however, η_{max} drops quickly by adding superfluous MnTe. Generally the output power densities of samples undergoing 3-h ball milling are higher than that of the pure $Bi_{0.52}Sb_{1.48}Te_3$. Overall, the 2-mol% MnTe sample undergoing 3-h ball milling has better thermoelectric performance than the others.

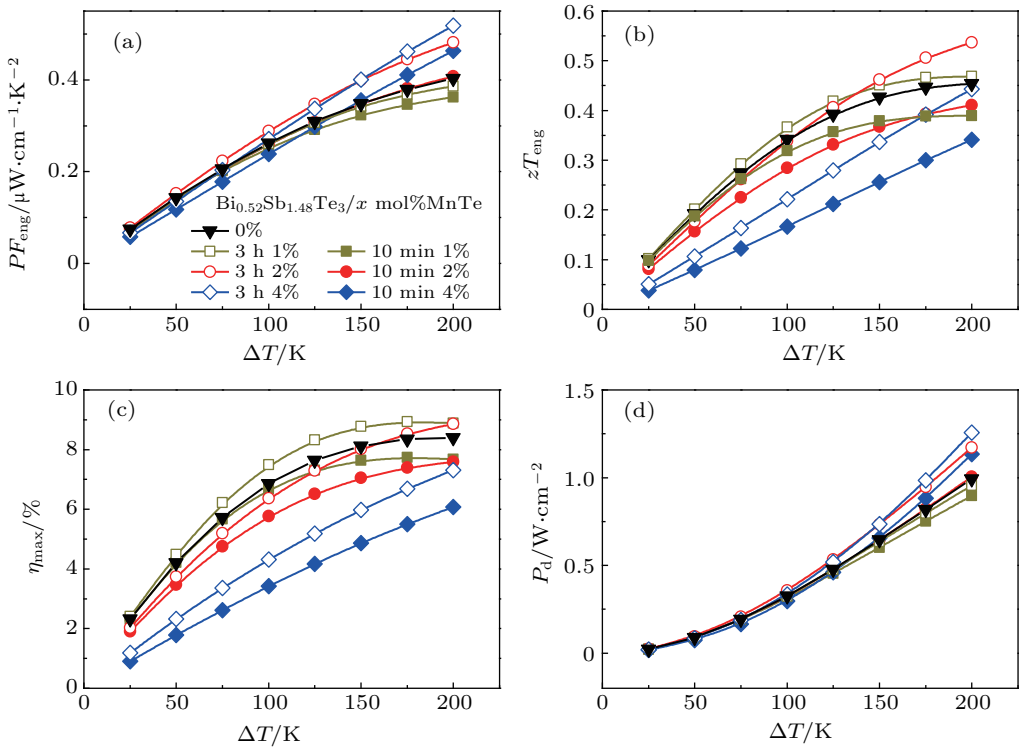


Fig. 6. (color online) Cumulative temperature dependence of (a) engineering power factor (PF_{eng}), (b) engineering figure of merit (zT_{eng}), (c) energy conversion efficiency (η), and (d) output power density (P_d).

4. Conclusions

In this work, a series of p-type $Bi_{0.52}Sb_{1.48}Te_3$/MnTe (0, 1, 2, and 4 mol%) nanocomposites are successfully fabricated through combined mechanical milling and spark plasma sintering process. The influence of MnTe second phase on the thermoelectric performance of $Bi_{0.52}Sb_{1.48}Te_3$ composite is investigated. It is observed that the power factor of the composite can be enhanced by optimizing the carrier concentration through partial Mn doping on the Bi sites. The lattice thermal conductivity of the composite can be significantly suppressed by the MnTe additive due to the high-density grain boundary in the composite. Overall, the peak zT of the 1-mol% sample undergoing 3-h ball milling reaches 1.37 at 348 K, which is a 10% improvement in comparison with 1.24 of $Bi_{0.52}Sb_{1.48}Te_3$. In addition, the 2-mol% sample undergoing 3-h ball milling exhibits higher zT than the pure $Bi_{0.52}Sb_{1.48}Te_3$ above 348 K, an enhancement of 20% on the $(zT)_{eng}$ was obtained when the temperature difference reaches 200 K. These results imply that the MnTe can be used as an additive in BiSbTe based materials for enhancing thermoelectric performance.

References

[1] Liu N, Luo X G and Zhang M L 2014 *Chin. Phys. B* **23** 080502
[2] Bell L E 2008 *Science* **321** 1457
[3] Chen G, Dresselhaus M S, Dresselhaus G, Fleurial J P and Caillat T 2003 *Int. Mater. Rev.* **48** 45
[4] Snyder G J and Toberer E S 2008 *Nat. Mater.* **7** 105
[5] Shuai J Mao J Song S Zhu Q Sun J, Wang Y, He R, Zhou J, Chen G, Sligh D J and Ren Z 2017 *Energy Environ. Sci.* **10** 799
[6] Zhu T, Liu Y, Fu C, Heremans J P, Snyder J G and Zhao X 2017 *Adv. Mater.* **29** 1605884
[7] Tan G J, Zhao L D and Kanatzidis M G 2016 *Chem. Rev.* **116** 12123
[8] Zhao Q Z and Zhang D L 2017 *Chin. Phys. Lett.* **34** 034207
[9] Delaire O, Ma J, Marty K, May A F, McGuire M A, Du M H, Singh D J, Podlesnyak A, Ehlers G, Lumsden M D and Sales B C 2011 *Nat. Mater.* **10** 614
[10] Kanatzidis M G 2010 *Chem. Mater.* **22** 648
[11] Sootsman J R, Chung D Y and Kanatzidis M G 2009 *Angew Chem. Int. Edit.* **48** 8616
[12] Suekuni K, Avila M A, Umeo K, Fukuoka H, Yamanaka S, Nakagawa T and Takabatake T 2008 *Phys. Rev. B* **77** 235119
[13] Venkatasubramanian R 2000 *Phys. Rev. B* **61** 3091
[14] Dresselhaus M S, Chen G, Tang M Y, Yang R G, Lee H, Wang D Z, Ren Z F, Fleurial J P and Gogna P 2007 *Adv. Mater.* **19** 1043
[15] Venkatasubramanian R, Siivola E, Colpitts T and O'Quinn B 2001 *Nature* **413** 597
[16] Poudel B, Hao Q, Ma Y, Lan Y C, Minnich A, Yu B, Yan X A, Wang D Z, Muto A, Vashaee D, Chen X Y, Liu J M, Dresselhaus M S, Chen G and Ren Z F 2008 *Science* **320** 634
[17] Ma Y, Hao Q, Poudel B, Lan Y C, Yu B, Wang D Z, Chen G and Ren Z F 2008 *Nano Lett.* **8** 2580
[18] Wu Z H, Xie H Q, Wang Y Y, Xing J J and Mao J H 2015 *Chin. Phys. Lett.* **32** 117303
[19] Li Y Y, Li D, Qin X Y, Yang X H, Liu Y F, Zhang J, Dou Y C, Song C J and Xin H X 2015 *J. Mater. Chem. C* **3** 7045
[20] Kim E B, Dharmaiah P, Shin D, Lee K H and Hong S J 2017 *J. Alloys Compd.* **703** 614
[21] Cao B L, Jian J K, Ge B H, Li S M, Wang H, Liu J and Zhao H Z 2017 *Chin. Phys. B* **26** 017202
[22] Jonson M and Mahan G D 1980 *Phys. Rev. B* **21** 4223
[23] May A F, Toberer E S, Saramat A and Snyder G J 2009 *Phys. Rev. B* **80** 125205
[24] Fistul' V I 1969 *Heavily doped semiconductors* (New York: Plenum Press) p. 418
[25] Tan G, Liu W, Chi H, Su X, Wang S, Yan Y, Tang X, Wong-Ng W and Uher C 2013 *Acta Mater.* **61** 7693
[26] Tan G, Wang S, Yan Y, Li H and Tang X 2012 *J. Alloys Compd.* **513** 328
[27] Wang S Y, She X Y, Zheng G, Fu F, Li H and Tang X F 2012 *J. Electron. Mater.* **41** 1091
[28] Xie H H, Wang H, Pei Y Z, Fu C G, Liu X H, Snyder G J, Zhao X B and Zhu T J 2013 *Adv. Funct. Mater.* **23** 5123
[29] May A F, Flage-Larsen E and Snyder G J 2010 *Phys. Rev. B* **81** 125205
[30] Kim H S, Liu W S, Chen G, Chua C W and Ren Z F 2015 *PNAS* **112** 8205
[31] Altenkirch E 1909 *Phys. Z.* **10** 560